analytical chemistry

pubs.acs.org/ac
Article

Miniaturization and Optimization of NMR Shimsets Allow Efficient Field Shimming

Hossein Esmaeilizadshali, Dominique Buyens, Jan Korvink,* and Mazin Jouda*

Cite This: https://doi.org/10.1021/acs.analchem.5c06167
Read Online

ABSTRACT: We present a finite element method (FEM)-based framework for the joint optimization of nuclear magnetic resonance (NMR) cells, encompassing both the radio frequency (RF) coil and integrated shim systems. This approach enables systematic design with respect to sensitivity, RF isolation, and magnetic field homogeneity, ensuring efficient operation under demanding high-field conditions. As a proof of concept, we demonstrate a four-channel parallel NMR spectroscopy probe, where each channel incorporates a stripline-based RF detector confined by ground planes for intrinsic shielding and reduced interchannel coupling. Localized shimsets (x, y, z, and z^2) are codesigned with the RF coils to achieve high field homogeneity within each sample volume. At a proton Larmor frequency of 650 MHz (15.2 T), the optimized detectors exhibit a quality factor (Q) of 53 and residual interchannel coupling between −25 dB and −80 dB. The integrated shim systems achieve line widths as low as 2.8 Hz and resolve selected J-couplings while operating with currents in the range of −3 mA to 16 mA. These results highlight the potential of FEM-guided NMR cell optimization for enabling advanced multichannel probe architectures.

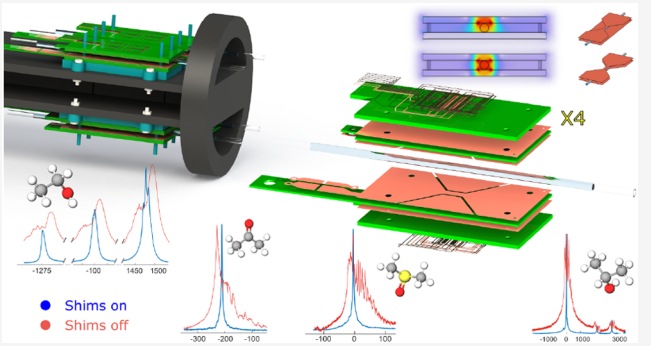

INTRODUCTION

Commercial NMR spectrometers are typically equipped with a single detector, restricting measurements to one sample at a time, making NMR spectroscopy a notably low-throughput technique. A number of attempts have been made to increase the throughput of NMR experiments by allowing the measurement of multiple samples simultaneously.[1−7] One of the early efforts in this field was the work by Fisher et al.,[1] who presented an NMR probe equipped with two RF coils to simultaneously measure the ^{13}C NMR signals from two samples in a 300 MHz NMR spectrometer. The achieved line width was approximately 9.2 Hz, allowing the J-coupling resolution. This probe was further developed by MacNamara et al. in 1999, who introduced a 4-coil probe capable of acquiring the signals from four samples simultaneously.[3] The four coils were connected in parallel in a single resonance circuit. Therefore, a gradient field along the z-axis was applied to assign a frequency offset to each signal, enabling the simultaneous acquisition of the four signals via a single RF receiver. In 2004, Wang et al.[8] demonstrated an eight-channel NMR array of micro solenoidal coils. The microcoils were placed in close proximity to each other so that they could all fit within the homogeneous volume of the field and could, as a result, be shimmed via a single shimming set. To reduce the effects of magnetic susceptibility jumps and consequently facilitate shimming, the microcoils were submerged in a container of FC-43, a nonconducting susceptibility-matching perfluorinated fluid. Despite their successful implementation and promising potential, these attempts lack generalizability due to the absence of localized shims integrated with each micro coil. Shimming systems available in commercial spectrometers are designed to homogenize the field over a limited specific volume around their center, where the shim profiles are symmetric. This imposes a strict limit on the number of NMR coils and requires them to be close to each other, raising the problem of RF coupling and signal crosstalk. Localized integrated shims[9−12] offer a promising solution to this generalizability problem. By tailoring magnetic field corrections to each detector volume, localized shims make it possible to design NMR arrays with many independent coils, limited mainly by the magnet bore size rather than by shim system constraints. One of the early attempts to integrate shims with the RF coil is the work by Van Meerten et al.,[9] in which a 16-channel 1D shim system was used to achieve a 2.2 Hz line width in a 144 MHz NMR magnet. This shim system is well-suited to correct sample-induced inhomogeneity of the

Received: October 3, 2025
Revised: April 14, 2026
Accepted: April 16, 2026

https://doi.org/10.1021/acs.analchem.5c06167
Anal. Chem. XXXX, XXX, XXX−XXX

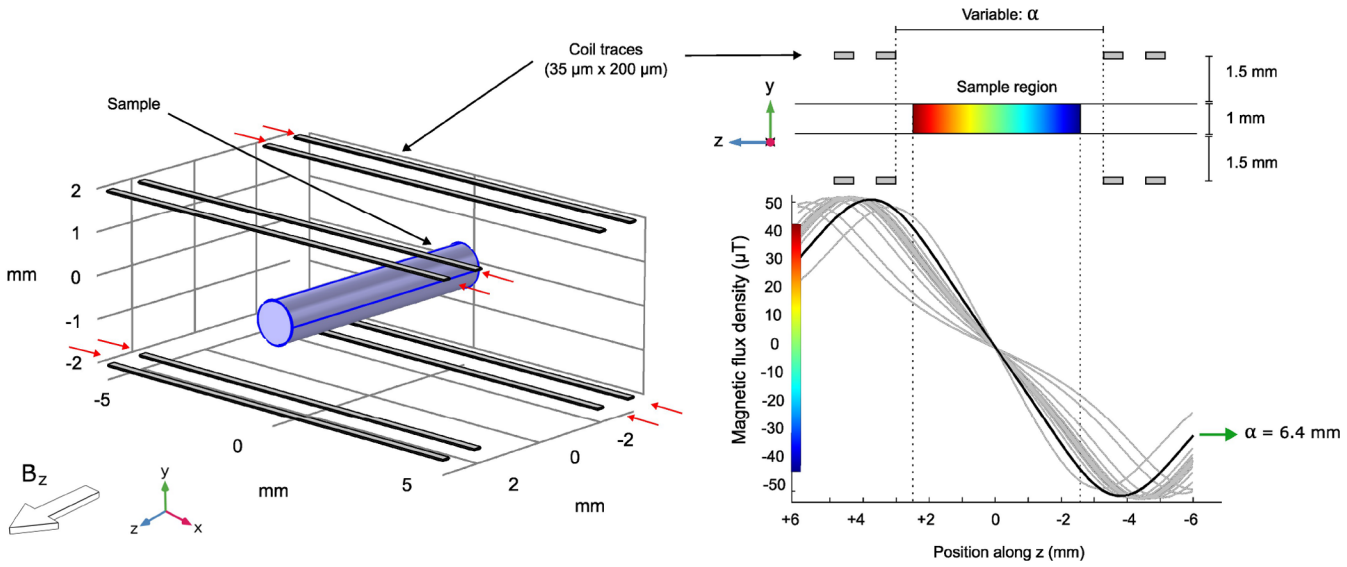

Figure 1. FEM-based optimization of a z-shim. **Left:** 3D schematic of the shim coil, illustrating the conductor layout and the sample region. The wire length is shown arbitrarily, as the underlying simulation was performed in the 2D *yz*-plane. **Right:** Optimization results, where the gray curves represent intermediate iterations and the black curve denotes the final solution after convergence.

static field B_0 for long samples extended along the *z*-axis with a narrow lateral extension. However, if the B_0 initially exhibits field gradients along the other axes, the 1D shim system will be insufficient. Additionally, the scalability of this shim system is limited due to the large number of shim currents needed. In a relatively recent work, Cheng et al.[10] demonstrated a two-cell NMR array with locally integrated linear shims, enabling the simultaneous measurement of two samples and highlighting the significance of localized shims in achieving high-throughput NMR. In a previous work by the authors,[12] the potential of optimizing the NMR cell—including sample geometry, RF coil, and integrated shims—as a unified unit was demonstrated by building an NMR cell with three linear shims (*x*, *y*, and *z*), capable of achieving a 4 Hz line width in a 1.05 T preclinical imaging magnet, thereby resolving the *J*-couplings. In this work, we advance this concept by introducing a finite element method (FEM)-based optimization framework for localized shim systems codesigned with their corresponding RF coils. FEM-based optimization allows systematic tailoring of shim geometries to maximize field homogeneity with minimal system complexity, while maintaining high coil sensitivity and low interchannel coupling. This approach establishes localized shims as the key enabler for scaling NMR into a high-throughput technique. As an application of this methodology, we demonstrate a four-channel NMR array operating at 15.2 T, capable of simultaneously analyzing four samples. The probe achieves sub-10 ppb spectral resolution using only three first-order shim elements, while crosstalk is mitigated through the use of inherently shielded stripline detectors and postprocessing of the acquired spectra. This demonstration highlights the transformative potential of FEM-optimized localized shims for enabling advanced, parallel NMR spectroscopy.

MATERIALS AND METHODS

Benchmark Samples

The samples used to benchmark and characterize the performance of the proposed hardware included ethanol, acetone, DMSO (dimethyl sulfoxide), and isopropanol. These solvents were selected to provide sufficiently high signal-to-noise ratios (SNRs), which are essential for reliable shimming. To demonstrate the applicability of our NMR sensor to real biological samples, we selected a series of natural and biologically relevant materials. Orange and tomato extracts were prepared from commercially available freeze-dried powders. For the orange extract, 50 mg of orange powder was dissolved in 1 mL of D_2O containing 100 mM 3-(trimethylsilyl)propionic-2,2,3,3-d_4 acid sodium salt (TSP-d_4) as an internal chemical shift reference. Tomato extract was prepared by dissolving 300 mg of tomato powder in 4 mL D_2O, centrifuging at 6000 rpm for 3 min to remove insoluble material, and subsequently adding TSP-d_4 to a final concentration of 50 mM. A cell-buffer-mimicking sample was prepared by first dissolving 86 mg TSP-d_4 in 5 mL D_2O to obtain a 100 mM stock solution, into which D-(+)-glucose was added to reach 100 mM concentration. Finally, a urine-based sample was obtained by dissolving 50 mg of lyophilized human urine in 1 mL D_2O containing 100 mM TSP-d_4, providing a representative complex biological mixture.

FEM-Based Shim Coil Optimization

Successful shimming requires shim coils capable of accurately reproducing the terms of a spherical harmonic expansion of the magnetic field within the sample.[13,14] This, in turn, demands precise positioning and alignment of the current-carrying coil segments relative to the sample volume. To address this challenge, we employed the optimization module of COMSOL Multiphysics to perform finite-element-method (FEM)-based simulations aimed at the design and optimization of shim coil geometries. Figure 1 shows an example of FEM-guided optimization for a z-shim, where an anti-Helmholtz coil is designed to produce a static magnetic field with a linear gradient along the *z*-axis. Each side of the anti-Helmholtz consists of two loops, separated by a variable distance α, which serves as the optimization parameter. The conductor width and intraloop spacing were both set to 200 mum, ensuring compatibility with standard printed circuit board (PCB) fabrication. Likewise, the spacing between the coil conductors and the sample region along the *y*-axis was set to 1.5 mm, corresponding to the standard PCB substrate thickness. The sample region was modeled as a cylinder with a diameter of 1 mm and a length of 5 mm, representing a capillary sample compatible with a stripline RF detector. The optimization objective was defined as minimizing the second derivative of the magnetic field along the *z*-axis, $\min(\partial^2 B_z(\alpha)/\partial z^2)$, thereby maximizing field linearity within the sample volume. The second derivative was evaluated over an extended region slightly larger than 5 mm to ensure that any residual nonlinearities fall outside the sample boundaries. The field linearity

https://doi.org/10.1021/acs.analchem.5c06167
Anal. Chem. XXXX, XXX, XXX−XXX

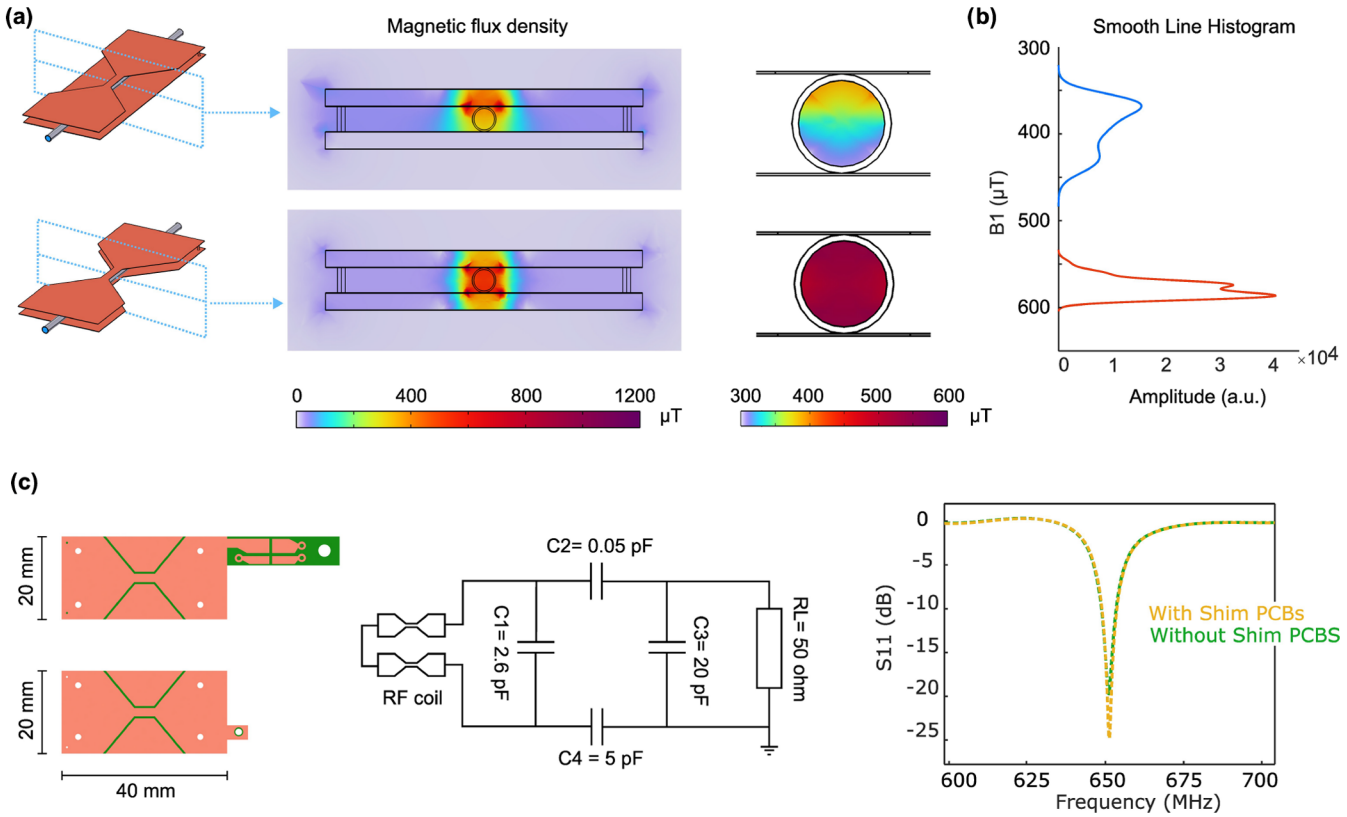

Figure 2. (a) A comparison between the conventional stripline (top) detector and the modified stripline used in this paper (bottom). (b) Field distribution in the sample shows a superior field strength and uniformity of the modified stripline. (c) RF circuit design and topology of tuning and matching capacitors, along with the S11 reflection curve of the modified stripline in two states to investigate the effect of shim coils on the S-parameter.

across the interval $-2.5 < z < +2.5$ (the sample region) was quantified using the normalized root-mean-square error (NRMSE) in MATLAB. The resulting deviation of only 0.16% demonstrates that the optimized anti-Helmholtz coil provides a highly linear z-shim.

System Design

The system presented here is designed to perform simultaneous NMR spectroscopy of four channels. Therefore, it consists of four cells, each of which includes an RF section to generate the resonant radio frequency magnetic field (B_1) at the Larmor frequency and shim coils to homogenize the B_0 in each sample. First, considering the RF section, a stripline topology was selected for the RF coil. As detailed in several papers,[9,15,16] in a stripline, the narrow section of the signal plane increases the current density and B_1 field in the sample region, thereby boosting the sensitivity. Even though other coil topologies, such as solenoidal or spiral coils, can produce a strong magnetic field, the susceptibility jumps resulting from their alignment with respect to B_0 make them less attractive, particularly in high-field systems. The stripline, on the contrary, suffers less from the susceptibility mismatches due to the parallel alignment of the sample and the coil to B_0. Another advantage of the stripline is the straightforward scalability enabled by its planar structure, making it readily adjustable to confine the sample, ensuring the strongest B_1-sample interaction and maximum filling factor. Another key feature of this coil, due to its planar shape, is the possibility to sandwich it between several layers, including, for instance, shim coils and grounded RF shields, which not only prevent the unwanted RF noise but also reduce the RF coupling between the adjacent channels.

The stripline structure introduced here is different from the conventional stripline structure.[15,17] Unlike the conventional stripline in which there is one signal plane sandwiched between two ground planes, the modified stripline comprises four layers, the outer of which are the ground planes, while the inner ones represent the signal planes between which the sample is placed. Having two signal planes with narrow sections boosts the B_1 field in the sample and makes it, at the same time, more uniform due to symmetry, as demonstrated in Figure 2. Such a high B_1 field homogeneity can be very useful for experiments using advanced pulse sequences.[18,19] The design of the stripline was based on the initial selection of a 1 mm glass capillary as the sample holder, ensuring a sample that is small enough to minimize B_0 inhomogeneities but still sufficiently large to maintain the high SNR required for shimming. Based on this selection, the width of the active section of the stripline was determined to be 2 mm, two times the diameter of the capillary to ensure high B_1 uniformity.[20] Even though slightly below the optimal length-to-width ratio demonstrated by Bart et al.,[20] the length of the stripline's active section was purposefully set to 5 mm to ensure a sufficiently large sample volume, hence a high SNR, but, at the same time, is not too long such that it resembles a one-dimensional structure that is far from the spherical shape whose field inhomogeneities can be nicely decomposed by a spherical harmonics expansion.[13,14]

To compare the performance of the conventional stripline coil with the modified design proposed in this study, Figure 2 presents the results of finite element modeling (FEM) simulations conducted using COMSOL Multiphysics (Electromagnetic Waves, Frequency Domain), highlighting differences in B_1 field strength and uniformity. The simulation results report a factor of 1.47 sensitivity boost and a field uniformity enhancement by a factor of 1.23 in comparison to the conventional stripline. The figure additionally shows the tuning and matching circuit employed along with the measured reflection curve, S11, of the manufactured stripline.

The central challenge, however, lies in shimming. Within each NMR cell, the magnetic field inhomogeneities can be expressed as a spherical harmonic expansion, an orthogonal basis that allows correction of individual terms without mutual interference.[13,14] While an infinite number of shim coils would be required to correct

https://doi.org/10.1021/acs.analchem.5c06167
Anal. Chem. XXXX, XXX, XXX−XXX

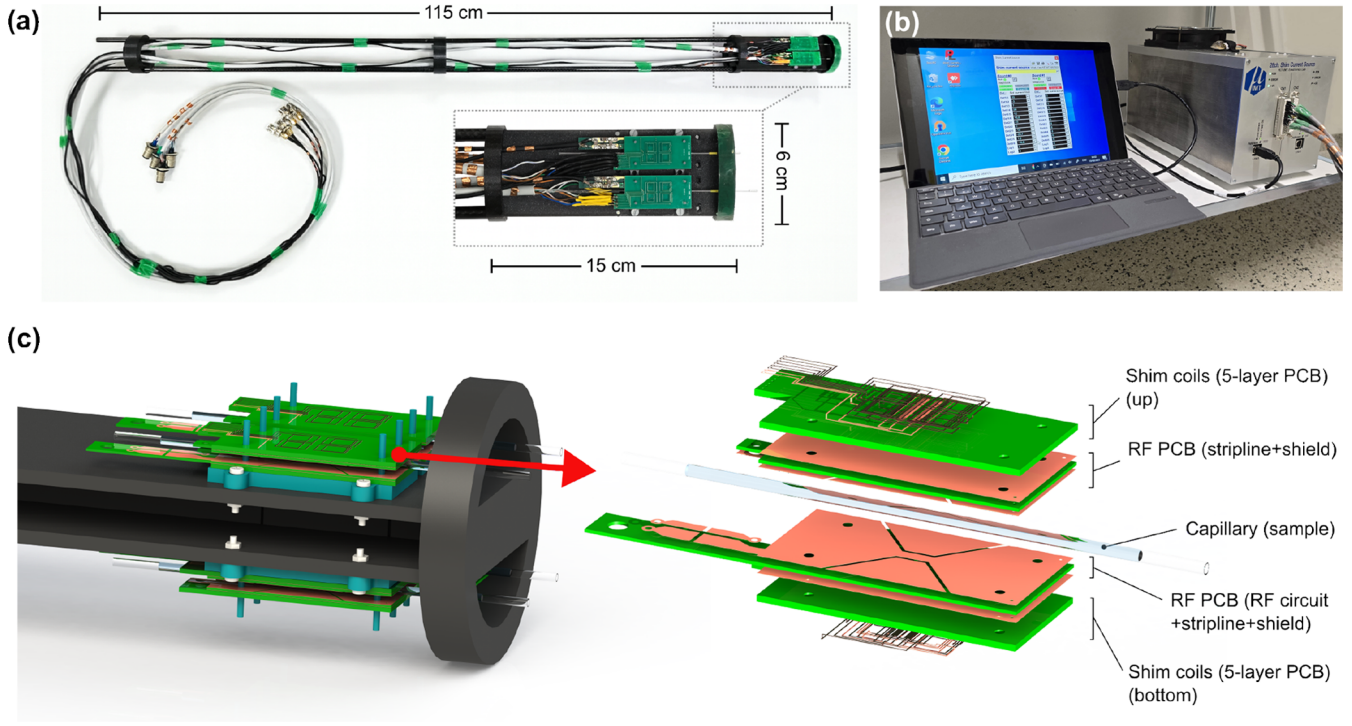

Figure 3. (a) The four-channel NMR probe with the RF and shim cables. (b) The home-built multichannel current source used to drive the shim coils. (c) An exploded view of a CAD model of the probe, highlighting the various metal and dielectric layers stacked to form the NMR cell.

all terms, practical field inhomogeneities are dominated by low-order variations. Accordingly, each cell in our prototype incorporates four shim elements: three linear terms (x, y, and z) and one quadratic term (z^2). This set strikes a balance between correction performance and system complexity by limiting the number of shim drivers and feedthroughs required. The shim geometries were first drafted in SolidWorks and then subjected to FEM-based optimization in COMSOL Multiphysics. Multiple design iterations were explored to maximize field fidelity, with trace widths fixed to 200 μm and thicknesses to 35 μm, consistent with standard PCB copper layers. The optimization targeted the placement of coil segments perpendicular to B_0, as these contribute directly to field generation along B_0. A key design criterion was to ensure that the intended field profile (linear or parabolic) was preserved across offsets within the sample region along other axes. After determining optimal segment placement, coil loops were completed with return traces parallel to B_0, ensuring negligible perturbation of the shim profile. Figure S1 summarizes the FEM simulation results for the complete shimset, showing the field distributions generated by the x, y, z, and z^2 coils under a DC excitation of 1 A. These results validate the ability of the FEM-optimized shimset to generate the required harmonic profiles with high fidelity, thereby enabling localized shimming as the central enabler of parallel high-throughput NMR spectroscopy.

Manufactured System

The probehead is made in such a way that it can accommodate four separate NMR cells side by side and also fit into the magnet's bore (diameter = 60 mm). During all the fabrication and assembly stages, we were very careful to utilize only nonmagnetic materials and components to avoid any potential B_0 disturbance. The probehead's mainframe, thus, was 3D printed using a PLA printer (Ultimaker 3), while the stripline support and alignment structure was 3D printed via an SLA printer (Prusa). Moreover, a silver surface finish was chosen for the PCBs to avoid the paramagnetic nickel, which is typically used with the gold-based surface finish. After assembling the stripline detectors, an ADS (Advanced Design System) simulation was carried out to calculate the tuning and matching capacitor values following the circuit topology shown in Figure 2. The simulations targeted a ^{1}H Larmor frequency of 650 MHz since the probe is designed to operate in a 15.2 T magnet. For tuning and matching the NMR detectors and due to space limitations, we decided to utilize discrete fixed-valued capacitors to avoid the bulky nonmagnetic trimmer capacitors. Therefore, the simulation results were accurate enough as a start, and we only needed a few soldering iterations to tune and match the four channels. After that, the shim PCBs were mounted below and above the striplines, and nonmagnetic Ethernet cables with an outer diameter of 5.4 mm were used to connect the shims.

As shim drivers, we utilized a homemade current source featuring 28 channels, each capable of delivering ± 300 mA with a high adjustment resolution of 16 bits and very low long-term thermal drift of 450 nA/°C. More details on the shim driver can be found in the paper by Becker et al.[21] To assess the performance of the parallel probe via ^{1}H NMR spectroscopy experiments, commonly available hydrogen-containing compounds were utilized as test samples. Ethanol, acetone, DMSO (dimethyl sulfoxide), and isopropanol samples were loaded into channels 1 to 4, respectively, by filling the 1 mm glass sample holders. To prevent evaporation, the capillaries were sealed after sample injection using separate syringes. UV-curable adhesive was applied to both ends of the capillary, ensuring a sufficient air gap between the sample and the glue to avoid any interaction. The adhesive was then solidified by exposure to UV light. Figure 3a shows an image of the assembled four-channel probe with the RF as well as the shim cables, whereas an exploded view of one of the NMR cells is illustrated in part c of the figure, showing the different layers of the stripline and shim coils and how they are stacked together. Figure 3b demonstrates, on the other hand, the homemade current source utilized for shimming along with the control software.

RESULTS

After assembling the 4-channel probe, we first carried out a characterization of the RF coupling between the channels through the measurement of the reflection parameters (S-parameters). For these measurements, we utilized a four-port vector network analyzer (Keysight E5071C ENA). For the coupling characterization, one can perform six possible S-

https://doi.org/10.1021/acs.analchem.5c06167
Anal. Chem. XXXX, XXX, XXX−XXX

parameter measurements representing the mutual coupling for all possible combinations; however, due to symmetry, we report here only three channels representing three possible configurations, namely, horizontally adjacent coils, vertically adjacent coils, and diagonal coils. Figure S2 shows the coils' configurations and the corresponding reflection, S_{ii}, as well as transmission, S_{ij}, parameters, reporting a −30 dB (3%), −68 dB (0.04%), and −19 dB (11%) for S_{23}, S_{24}, and S_{34}, respectively.

Individual Channels Testing

All NMR measurements presented in this study were conducted using a 15.2 T preclinical MRI scanner (Bruker BioSpec), corresponding to a 650 MHz Larmor frequency for ^{1}H, and equipped with four ^{1}H/^{19}F and four broadband RF transceiver channels. This magnet offers high SNR, but at the same time, higher sensitivity to susceptibility changes. Data acquisition was performed using ParaVision 360, Bruker's standard NMR imaging software, while signal processing and data visualization were carried out in MATLAB. For the NMR experiments, excitation pulses of 85 μs duration were employed, corresponding to a bandwidth of 15 kHz. The acquisition bandwidth was set to 15 kHz, with a total acquisition time of 1 s. The RF excitation power was manually adjusted to 2.5 W to achieve a 90° flip angle.

To evaluate the performance of the local shim coils relative to the global shims provided by the commercial system, we first conducted an NMR experiment on each channel with all local shim coils turned off. An automatic shimming routine was then performed using the global shim set—including both first- and second-order shim coils—to optimize magnetic field homogeneity for the sample in each channel. Once the global autoshimming procedure had converged and completed, we acquired the NMR spectrum and subsequently set all global shim currents to zero. We then manually shimmed the same sample on the same channel using the local shim coils powered by the custom-built current source. As an example, Figure S3 presents a comparison of the results obtained with global and local shimming, demonstrating nearly identical shimming performance and achieved line widths. In both cases, the J-couplings of the CH_3 group in the samples were clearly resolved. Additionally, Figure S4 compares the performance of the FEM-optimized NMR cell with that of a commercial 500 MHz NMR spectrometer using the same sample and the same number of shims, demonstrating the superior performance of the NMR cell.

To determine the limit of detection (LoD) of the NMR sensor, a series of NMR spectroscopy experiments was performed on a 4 μL sample of pyrazine dissolved in D_2O at concentrations of 100 mM, 50 mM, 20 mM, and 10 mM. All measurements were carried out using a 90° excitation pulse with a transmit power of 2.5 W, an acquisition duration of 260 ms, and 64 signal averages.

The resulting spectra, shown in Figure 4, exhibit signal-to-noise ratio (SNR) values of 85, 47, 20, and 12 for the pyrazine resonance at 8.66 ppm, respectively. To obtain a conservative estimate of the LoD, the lowest SNR-per-concentration ratio was considered, corresponding to an SNR of 85 at a concentration of 100 mM. Assuming a minimum detectable SNR of 3, the concentration LoD for a single scan can be estimated as

$$c_{\mathrm{LoD}} = \frac{3\sqrt{64}}{85/100} \approx 30\ \mathrm{mM}$$

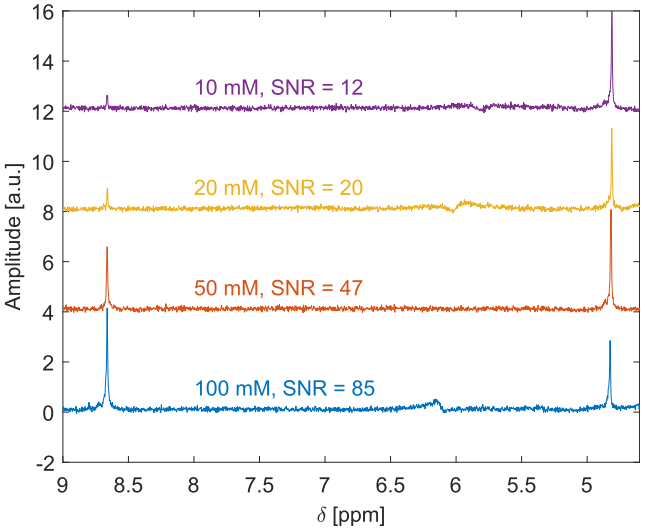

Figure 4. NMR spectra of pyrazine dissolved in D_2O at multiple concentrations, acquired with 64 signal averages to evaluate the limit of detection (LoD) of the NMR sensor.

For a sample volume of 4 μL, this concentration corresponds to an amount of substance of

$$n = 30 \times 10^{-3} \cdot 4 \times 10^{-6} = 120\ \mathrm{nmol}$$

Four-Channel NMR Experiments

Following the successful NMR measurement on a single channel using only the localized shims, we extended the experiment to simultaneously accommodate four channels, each containing a different sample: ethanol, acetone, DMSO, and isopropanol. We began by configuring a new probe setup in ParaVision, where the four NMR cells were connected to the four narrow-band ^{1}H/^{19}F transceive channels of the Bruker spectrometer. This setup enabled us to run the same NMR sequence across all channels in full synchronization. Subsequently, we performed manual shimming of the localized shim coils on all four channels while running a single-pulse experiment in parallel. The manual shimming process for all channels took approximately 90 min. We concluded the shimming once we achieved spectral resolutions comparable to those obtained with global shimming on a single channel.

The upper part of Figure 5 depicts the four NMR spectra acquired simultaneously. The line widths of singlets achieved using the localized shims ranged from 2.8 to 4.5 Hz, enabling clear resolution of the J-couplings in the ethanol and isopropanol samples. The lower part of Figure 5, on the other hand, demonstrates the effect of turning off the localized shims on the concurrently acquired NMR spectra.

An example of NMR spectroscopy of four natural and biological samples beyond simple solvents is illustrated in Figure 6. These samples include orange and tomato extracts prepared from freeze-dried powders, a cell-buffer-mimicking sample, and a urine-based sample. The sample preparation steps are detailed in the section "Benchmark Samples" section.

Post Processing. Despite all the measures we took to ensure minimum coupling between the cells, during the experiments, we could still recognize a notable coupling between the channels, ranging from −19 dB to −68 dB. To eliminate this crosstalk, we developed an optimization-based algorithm that processes the collected data to determine the mutual coupling coefficients during the NMR experiment. The

https://doi.org/10.1021/acs.analchem.5c06167
Anal. Chem. XXXX, XXX, XXX−XXX

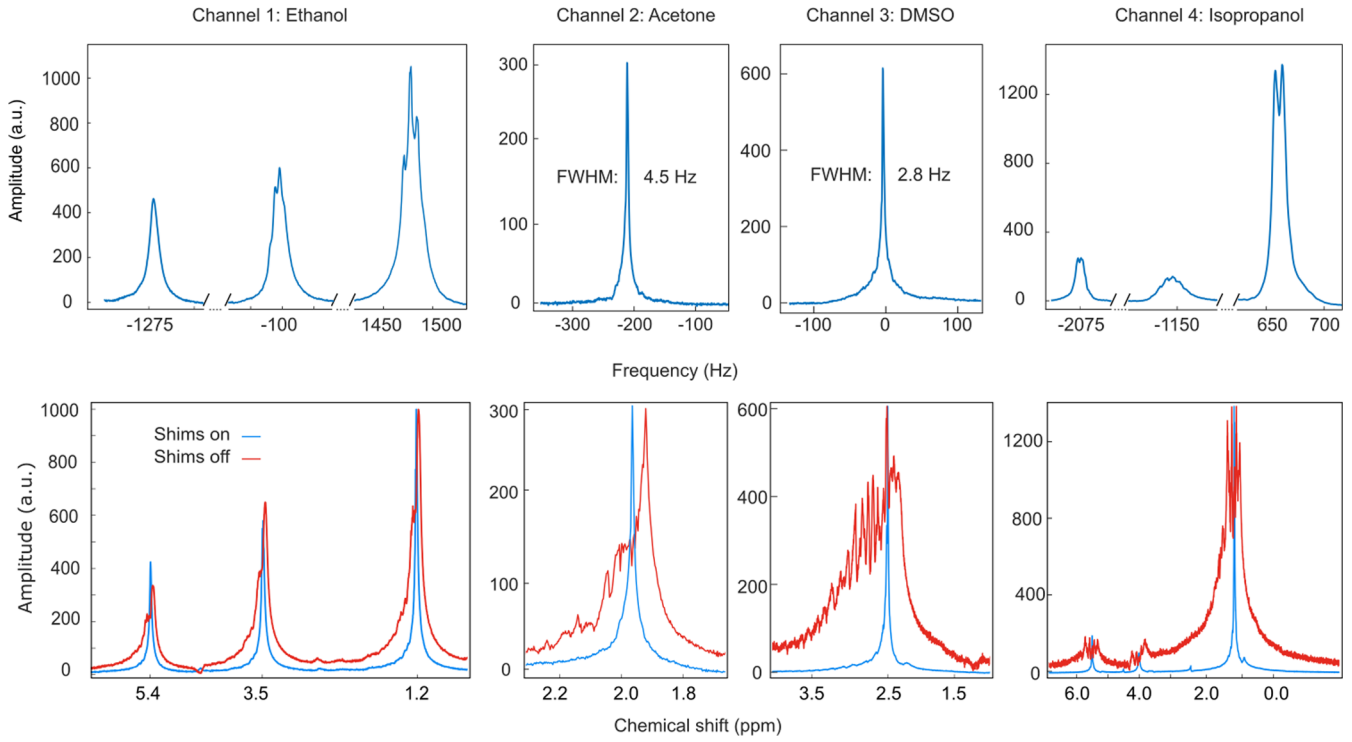

Figure 5. Upper: Results of a parallel NMR experiment of four different samples simultaneously measured. The shimming in this experiment was done using the localized shims only (global shims are off). Lower: Effect of turning the localized shims off.

algorithm utilizes a reference data set of the four NMR spectra collected individually, representing the ideal case. For simplicity, we first considered the magnitude of the NMR spectra (as in Figure S3). The algorithm works as follows: let S_i, with $i \in [1, 4]$, be the magnitude of the i-th ideal spectrum, and suppose that S_i', with $i \in [1, 4]$, is the magnitude of the i-th spectrum collected simultaneously with the other three. The corrected i-th spectrum, S_i'', is then calculated as

$$S_i'' = S_i' - \sum_k c_k \cdot S_k', \quad \text{with } k \in [1, 4] \text{ and } k \neq i \tag{1}$$

where c_k, the optimization variable, represents the coupling coefficient between the i-th and k-th spectra. The following optimization objective was used to find the coupling coefficients.

$$\min\left\{\sum (S_i'' - S_i)^2\right\} \tag{2}$$

Extending the postprocessing decoupling method to the real spectra ($\Re$), as in Figure 5, makes the optimization problem quite more sophisticated, as six more optimization variables must be included, representing the zero- and first-order phases of the coupled spectra. In this case, if S_i is the complex interpretation of the i-th ideal spectrum and S_i' is the complex form of the i-th spectrum collected simultaneously with the other three, then the complex form the i-th corrected spectrum, S_i'', is calculated as

$$S_i'' = S_i' - \sum_k c_k \cdot S_k' \cdot e^{j(\phi_{0,k} + \phi_{1,k} f)}, \text{ with } k \in [1, 4] \text{ and } k \neq i \tag{3}$$

where $\phi_{0,k}$ and $\phi_{1,k}$ are the zero- and first-order phases of the coupling from the k-th spectrum. The optimization objective becomes

$$\min\left\{\sum (\Re\{S_i''\} - \Re\{S_i\})^2\right\} \tag{4}$$

Figure S5 demonstrates the application of the decoupling algorithm on the spectrum of channel 4, showing a significant reduction (more than 70%) of the amplitudes of the coupled peaks.

Effect of Shim Stray Fields

Another key aspect evaluated was the impact of the stray field from a localized shimset on adjacent samples. Minimizing this influence is crucial to ensure that the shimming of each sample remains independent of the conditions of neighboring samples, thereby accelerating the overall shimming process. Figure S6 illustrates the influence of the shim coils on neighboring channels in both horizontal and vertical directions.

Horizontally, the shim coils of channel 2 had virtually no effect on the spectral resolution of channel 1, with both exhibiting a similar line width and j-coupling resolution. The only observable difference was a minor frequency shift of approximately 3 Hz. Vertically, the impact of channel 2's shim coils on the spectrum of channel 3 was also examined. Here again, the spectral resolution remained unaffected (FWHM: 2.8 Hz for both cases), with a slight frequency shift of about 6 Hz. These results highlight the highly localized nature of the shim coils and their close proximity to their respective samples, which effectively confines their influence to a small region and renders the stray fields nearly negligible. Finally, Figures S7 and S8 illustrate the effectiveness of the localized shims integrated into the NMR cell in preserving high-quality shimming independent of the sample position.

DISCUSSION AND CONCLUSIONS

The results presented here demonstrate how FEM-based optimization of the combined RF coil and shimset enables

https://doi.org/10.1021/acs.analchem.5c06167
Anal. Chem. XXXX, XXX, XXX−XXX

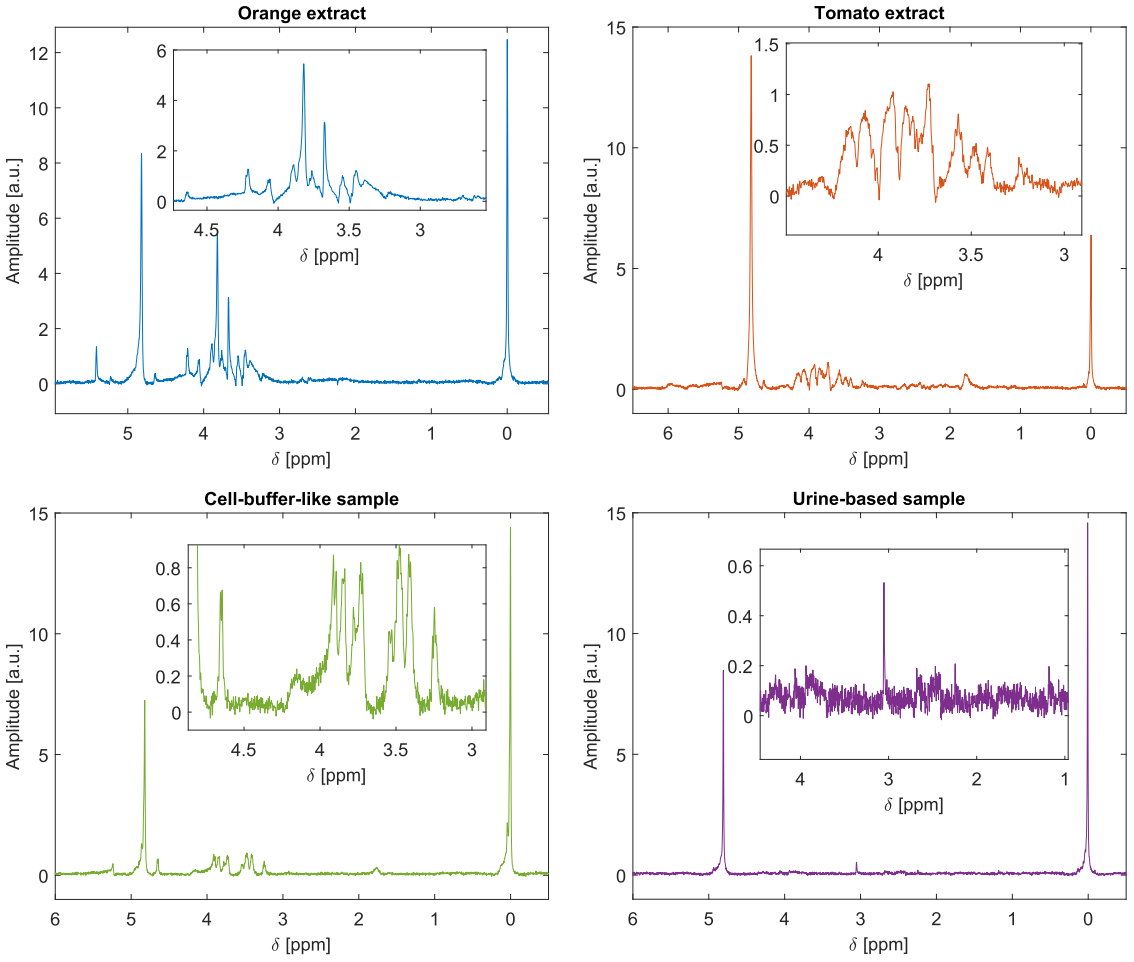

Figure 6. ^{1}H NMR spectra of four samples: reconstituted orange and tomato extracts prepared from freeze-dried powders, a cell-buffer-mimicking sample, and a urine-based sample. The spectra were acquired using a 2.5 W 90° excitation pulse, an acquisition time of 260 ms, a 15 kHz spectral bandwidth, and 256 signal averages.

high-field parallel NMR spectroscopy with *J*-coupling resolution. By integrating a modified stripline detector with a localized shimset and treating the NMR cell as a single optimized unit, the system attains both strong and homogeneous B_1 fields and effective B_0 homogenization. This FEM-based optimization, carried out in COMSOL Multiphysics, allowed smart and efficient shims, with *x*, *y*, *z*, and z^2 only, to be sufficient to resolve the *J*-couplings in the samples. Although four localized shims (*x*, *y*, *z*, and z^2) were integrated with each detector, the experimental results showed that only the linear shims were effectively capable of correcting the majority of the field inhomogeneities and achieving *J*-couplings resolution. Even though we did not apply any postprocessing on the spectra to improve their line widths, methods such as the reference deconvolution[4,22] or recently developed AI-based methods[23,24] can be straightforwardly applied to further enhance the spectral resolution. This contribution presents a significant step toward high-throughput NMR spectroscopy. It has the full potential for further upscaling. Although we used, in this study, a 1 mm sample capillary to ensure a strong signal-to-noise ratio and ease of cell manufacturability using commercial PCB technology, the cells can be readily further miniaturized by applying clean-room and micromanufacturing technologies to achieve further upscaling. The localized nature of the shims makes their stray fields very small, thereby increasing the orthogonality between the cells and consequently making the shimming process faster. This is deeply in favor of further upscaling and ever higher throughput. Deep learning-based shimming methods,[21,25] recently developed by our group, can be exploited to automate the parallel shimming process and significantly reduce shimming time. A major concern that was partially addressed in this paper but is still remaining is the crosstalk between the cells. We addressed this through two approaches: first, using a hardware approach, by sandwiching the stripline detector between two ground planes to minimize the B_1 outside the detector, thereby reducing the RF coupling. The second approach was software-based, employing an optimization-based postprocessing algorithm to quantify the coupling between the channels through comparison with a reference set of spectra, and then subtracting this coupling. This can be further enhanced by applying field gradients to shift the frequencies of the cells so that they are out of each other's band, as shown by Hou et al.[4] The hardware complexity associated with high-throughput multicoil NMR, namely, the need for multiple RF transceivers, can be readily overcome using digital lock-in detection techniques such as the one described by our team earlier.[12] This digital multifrequency lock-in can be directly applied if the coils are tuned to address different nuclei. Otherwise, if all coils are tuned at the same Larmor frequency, then their signals can be frequency-multiplexed[26] before they are acquired via a single digital lock-in channel.

https://doi.org/10.1021/acs.analchem.5c06167
Anal. Chem. XXXX, XXX, XXX−XXX

■ ASSOCIATED CONTENT

Data Availability Statement

The data set supporting the findings of this study is available via KITopen at 10.35097/9q4576u57a6ju51t.

Supporting Information

The Supporting Information is available free of charge at https://pubs.acs.org/doi/10.1021/acs.analchem.5c06167.

> Additional details on the design, simulation, and experimental validation of the localized shim system. This includes FEM-simulated shim field profiles for the optimized shim coils (X, Y, Z, and Z^2), RF characterization of the probe in terms of matching and interchannel coupling, and comparative studies between local and global shimming performance. Further results demonstrate benchmarking against a commercial high-field NMR spectrometer, analysis of interchannel signal coupling and its mitigation, evaluation of stray field effects between neighboring channels, and validation of position- and orientation-independent shimming performance (PDF)

■ AUTHOR INFORMATION

Corresponding Authors

Jan Korvink − *Institute of Microstructure Technology, Karlsruhe Institute of Technology, D-76344 Eggenstein-Leopoldshafen, Germany*; orcid.org/0000-0003-4354-7295; Email: jan.korvink@kit.edu

Mazin Jouda − *Institute of Microstructure Technology, Karlsruhe Institute of Technology, D-76344 Eggenstein-Leopoldshafen, Germany*; orcid.org/0000-0002-1226-1174; Email: mazin.jouda@kit.edu

Authors

Hossein Esmaeilizadshali − *Institute of Microstructure Technology, Karlsruhe Institute of Technology, D-76344 Eggenstein-Leopoldshafen, Germany*

Dominique Buyens − *Institute of Microstructure Technology, Karlsruhe Institute of Technology, D-76344 Eggenstein-Leopoldshafen, Germany*

Complete contact information is available at: https://pubs.acs.org/10.1021/acs.analchem.5c06167

Notes

The authors declare the following competing financial interest(s): J.G.K. is a shareholder of Voxalytic GmbH, a startup company that produces microscale NMR devices. The other authors declare no competing interests.

■ ACKNOWLEDGMENTS

This work was funded by the Deutsche Forschungsgemeinschaft (DFG)—Project-ID 454252029—SFB/CRC 1527 (HyPERiON). This work was additionally supported by the Helmholtz Association Research Area Information, Materials Systems Engineering, Topic 5 Materials Information Discovery, Deutsche Forschungsgemeinschaft (DFG)—Project-ID 459819582—SFB 1537 (ECOSENSE), and the Karlsruhe Institute of Technology. The authors sincerely thank Mr. Achim Voigt for his support with the shim current source, and Dr. Jing Yang, Dr. Sylwia Barker, and Mr. Simon Fleischer for their assistance with sample preparation. The authors additionally acknowledge the KIT-Publication Fund.

■ REFERENCES

(1) Fisher, G.; Petucci, C.; MacNamara, E.; Raftery, D. NMR probe for the simultaneous acquisition of multiple samples. *J. Magn. Reson.* **1999**, *138* (1), 160−163, DOI: 10.1006/jmre.1999.1725.

(2) Li, Y.; Wolters, A.; Malawey, P.; Sweedler, J.; Webb, A. Multiple solenoidal microcoil probes for high-sensitivity, high-throughput nuclear magnetic resonance spectroscopy. *Anal. Chem.* **1999**, *71*, 4815−4820.

(3) MacNamara, E.; Hou, T.; Fisher, G.; Williams, S.; Raftery, D. Multiplex sample NMR: an approach to high-throughput NMR using a parallel coil probe. *Anal. Chim. Acta* **1999**, *397*, 9−16.

(4) Hou, T.; MacNamara, E.; Raftery, D. NMR analysis of multiple samples using parallel coils: improved performance using reference deconvolution and multidimensional methods. *Anal. Chim. Acta* **1999**, *400*, 297−305.

(5) Zhang, X.; Sweedler, J.; Webb, A. A probe design for the acquisition of homonuclear, heteronuclear, and inverse detected NMR spectra from multiple samples. *J. Magn. Reson.* **2001**, *153*, 254−258.

(6) Macnaughtan, M. A.; Hou, T.; MacNamara, E.; Santini, R. E.; Raftery, D. NMR difference probe: a dual-coil probe for NMR difference spectroscopy. *J. Magn. Reson.* **2002**, *156*, 97−103.

(7) Macnaughtan, M. A.; Hou, T.; Xu, J.; Raftery, D. High-throughput nuclear magnetic resonance analysis using a multiple coil flow probe. *Anal. Chem.* **2003**, *75*, 5116−5123.

(8) Wang, H.; Ciobanu, L.; Edison, A.; Webb, A. An eight-coil high-frequency probehead design for high-throughput nuclear magnetic resonance spectroscopy. *J. Magn. Reson.* **2004**, *170*, 206−212.

(9) van Meerten, S. G. J.; van Bentum, P. J. M.; Kentgens, A. P. Shim-on-chip design for microfluidic NMR detectors. *Anal. Chem.* **2018**, *90*, 10134−10138.

(10) Cheng, Y.-T.; Jouda, M.; Korvink, J. Sample-centred shimming enables independent parallel NMR detection. *Sci. Rep.* **2022**, *12*, No. 14149.

(11) Becker, M.; Jouda, M.; Kolchinskaya, A.; Korvink, J. G. Deep regression with ensembles enables fast, first-order shimming in low-field NMR. *J. Magn. Reson.* **2022**, *336*, No. 107151.

(12) Esmaeilizadshali, H.; Lehmkuhl, S.; Korvink, J.; Jouda, M. Localized Shims Enable Low-Field Simultaneous Multinuclear NMR Spectroscopy. *Anal. Chem.* **2024**, *96*, 17201−17208.

(13) Golay, M. J. E. Field homogenizing coils for nuclear spin resonance instrumentation. *Rev. Sci. Instrum.* **1958**, *29*, 313−315.

(14) Roméo, F.; Hoult, D. I. Magnet field profiling: Analysis and correcting coil design. *Magn. Reson. Med.* **1984**, *1*, 44−65.

(15) van Bentum, P.; Janssen, J.; Kentgens, A.; Bart, J.; Gardeniers, J. Stripline probes for nuclear magnetic resonance. *J. Magn. Reson.* **2007**, *189*, 104−113.

(16) Oosthoek-de Vries, A. J.; Bart, J.; Tiggelaar, R. M.; Janssen, J. W. G.; van Bentum, P. J. M.; Gardeniers, H. J. G. E.; Kentgens, A. P. M. Continuous Flow 1H and 13C NMR Spectroscopy in Microfluidic Stripline NMR Chips. *Anal. Chem.* **2017**, *89*, 2296−2303.

(17) Zhang, X.; Ugurbil, K.; Chen, W. Microstrip RF surface coil design for extremely high-field MRI and spectroscopy. *Magn. Reson. Med.* **2001**, *46*, 443−450.

(18) Levitt, M. H.; Freeman, R. NMR population inversion using a composite pulse. *J. Magn. Reson.* **1979**, *33*, 473−476.

(19) Ibrahim, T. S.; Tang, L. Insight into RF power requirements and B field homogeneity for human MRI via rigorous FDTD approach. *J. Magn. Reson. Imaging* **2007**, *25*, 1235−1247.

(20) Bart, J.; Janssen, J.; Van Bentum, P.; Kentgens, A.; Gardeniers, J. G. Optimization of stripline-based microfluidic chips for high-resolution NMR. *J. Magn. Reson.* **2009**, *201*, 175−185.

(21) Becker, M.; Cheng, Y.-T.; Voigt, A.; Chenakkara, A.; He, M.; Lehmkuhl, S.; Jouda, M.; Korvink, J. G. Artificial intelligence-driven shimming for parallel high field nuclear magnetic resonance. *Sci. Rep.* **2023**, *13*, No. 17983.

(22) Metz, K.; Lam, M.; Webb, A. Reference deconvolution: a simple and effective method for resolution enhancement in nuclear magnetic resonance spectroscopy. *Concepts Magn. Reson.* **2000**, *12*, 21−42.
(23) Schmid, N.; Bruderer, S.; Paruzzo, F.; Fischetti, G.; Toscano, G.; Graf, D.; Fey, M.; Henrici, A.; Ziebart, V.; Heitmann, B.; et al. Deconvolution of 1D NMR spectra: A deep learning-based approach. *J. Magn. Reson.* **2023**, *347*, No. 107357.
(24) Jopa, S.; Bukowicki, M.; Shchukina, A.; Kazimierczuk, K. ShimNet: A Neural Network for Postacquisition Improvement of NMR Spectra Distorted by Magnetic-Field Inhomogeneity. *J. Phys. Chem. B* **2025**, DOI: 10.1021/acs.jpcb.5c02632.
(25) Becker, M.; Lehmkuhl, S.; Kesselheim, S.; Korvink, J. G.; Jouda, M. Acquisitions with random shim values enhance AI-driven NMR shimming. *J. Magn. Reson.* **2022**, *345*, No. 107323.
(26) Jouda, M.; Gruschke, O. G.; Korvink, J. G. Implementation of an in-field CMOS frequency division multiplexer for 9.4 T magnetic resonance applications. *Int. J. Circuit Theory Appl.* **2015**, *43*, 1861−1878.

https://doi.org/10.1021/acs.analchem.5c06167
Anal. Chem. XXXX, XXX, XXX−XXX